Immunity, Volume *56*

Supplemental information

Leveraging vaccination-induced protective antibodies to define conserved epitopes on influenza N2 neuraminidase

Ruipeng Lei, Wooseob Kim, Huibin Lv, Zongjun Mou, Michael J. Scherm, Aaron J. Schmitz, Jackson S. Turner, Timothy J.C. Tan, Yiquan Wang, Wenhao O. Ouyang, Weiwen Liang, Joel Rivera-Cardona, Chuyun Teo, Claire S. Graham, Christopher B. Brooke, Rachel M. Presti, Chris K.P. Mok, Florian Krammer, Xinghong Dai, Ali H. Ellebedy, and Nicholas C. Wu

Table S1. Cryo-EM data collection, refinement and validation statistics, Related to Figure 1.

	Mos99 NA+1F04 (EMDB-28729) (PDB 8EZ7)	Mos99 NA+3A10 (EMDB-28728) (PDB 8EZ3)	Mos99 NA+3C08 (EMDB-28730) (PDB 8EZ8)
Data collection and processing			
Magnification	130,000	130,000	130,000
Voltage (kV)	300	300	300
Electron exposure (e^{-}/Å^2)	50	50	50
Defocus range (μm)	-0.8 to -1.5	-0.8 to -1.5	-0.8 to -1.5
Pixel size (Å)	1.06	1.06	1.06
Symmetry imposed	C4	C4	C4
Initial particle images (no.)	707,915	338,116	895,207
Final particle images (no.)	480,812	216,485	230,209
Map resolution (Å)	2.63	2.5	2.78
FSC threshold 0.143			
Map resolution range (Å)	N/A		
Refinement			
Initial model used (PDB code)	7U4F	7U4F	7U4F
Model resolution (Å)	Up to 2.6	Up to 2.7	Up to 2.8
FSC threshold			
Model resolution range (Å)			
Map sharpening *B* factor (Å^2)	118.9	92.4	101.7
Model composition			
Non-hydrogen atoms	4927	4894	4847
Protein residues	624	631	630
Ligands			
B factors (Å^2)			
Protein			
Ligand			
R.m.s. deviations			
Bond lengths (Å)	0.003	0.004	0.003
Bond angles (°)	0.509	0.538	0.513
Validation			
MolProbity score			
Clashscore	7.8	8.19	10.06
Poor rotamers (%)	0.94	4.85	1.70
Ramachandran plot			
Favored (%)	97.25 %	95.94 %	95.77 %
Allowed (%)	2.75 %	4.06 %	4.07 %
Disallowed (%)	0.00 %	0.00 %	0.16 %

Table S2. Antibody escape mutations in N2 NA, Related to Figure 1.

N2 residues with antibody escape mutations	References
199	[S1]
69, 150, 198, 199, 220, 221, 253, 329, 334, 344, 368, 370, 403	[S2]
221, 290	[S3]
199, 258, 272	[S4]
338, 198, 199	[S5]
221, 248, 429	[S6]
245, 247, 468	[S7]
222, 227	[S8]

Table S3. Structures of antibodies in complex with NA in Protein Data Bank (PDB), Related to Figure 1.

PDB entry	Description	Reference
1NCA	Tern, H11N9+Fab NC41	[S9]
1NCD	Whale, H13N9+Fab NC41	[S9]
1NCB	Tern, H11N9+Fab NC41, mutant	[S10]
1NCC	Tern, H11N9+Fab NC41, mutant	[S10]
1NMA	Whale, H13N9+Fab NC10, mutant	[S11]
1NMB	Whale, H13N9+Fab NC10	[S12]
1A14	Tern, H11N9+NC10-Fv	[S13]
1NMC	Tern, H11N9+Single-chain antibody NC10	[S13]
2AEP	Memphis93, H3N2+Fab Mem5, 2.1A	[S14]
2AEQ	Memphis93, H3N2+Fab Mem5, 3A	[S14]
4QNP	A(H1N1)pdm09, H1N1+Fab CD6	[S15]
6N6B	Minnesota10, H3N2+Fab B10	[S7]
6PZY	Shanghai13, H7N9+Fab NA-73	[S16]
6PZZ	Shanghai13, H7N9+Fab NA-80	[S16]
6PZF	Hunan16, H7N9+Fab NA63	[S16]
6U02	Shanghai13, H7N9+Fab NA-63	[S16]
6PZW	Shanghai13, H7N9+Fab NA-22	[S16]
6PZE	Shanghai13, H7N9+Fab NA-45	[S16]
6Q20	Japan57, H2N2+Fab 1E01	[S17]
6Q23	Cal09, H1N1+Fab 1G01	[S17]
6Q1Z	Hunan16, H7N9+Fab 1G04	[S17]
6LXI	Brevig Mission1918, H1N1+Fab Z2B3	[S18]
6LXK	Serbia14, H1N1+Fab Z2B3-D102R	[S18]
6LXJ	Anhui13, H7N9+Fab Z2B3	[S18]
6V4N	B/Phuket13,IVB+Fab 1G05	[S19]
6V4O	B/Phuket13,IVB+20E1 Fab	[S19]

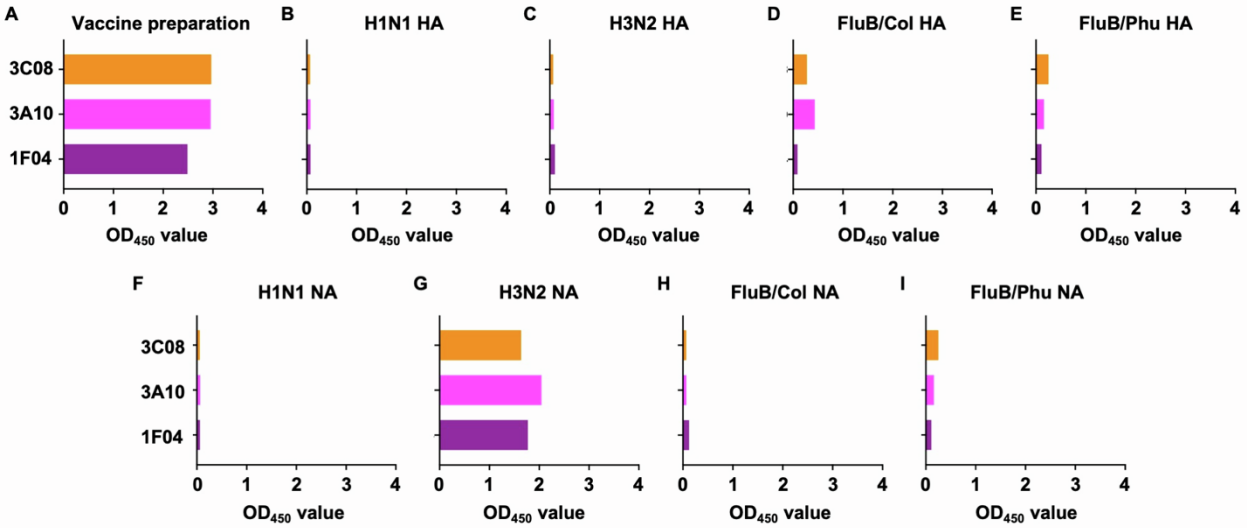

Figure S1. Determining the specificity of three antibodies from a vaccinee, Related to Table 1. Using ELISA, the binding of antibodies 3C08, 3A10, and 1F04 was tested against **(A)** the Flucelvax vaccine preparation for the 2019-2020 influenza season, **(B)** A/Brisbane/2/2018 (H1N1) HA, **(C)** A/Kansas/14/2017 (H3N2) HA, **(D)** B/Colorado/6/2017 (FluB/Col) HA, and **(E)** B/Phuket/3073/2013 (FluB/Phu) HA, **(F)** A/California/7/2009 (H1N1) NA, **(G)** A/Hong Kong/4801/2014 (H3N2) NA, **(H)** B/Colorado/6/2017 (FluB/Col) NA, and **(I)** B/Phuket/3073/2013 (FluB/Phu) NA.

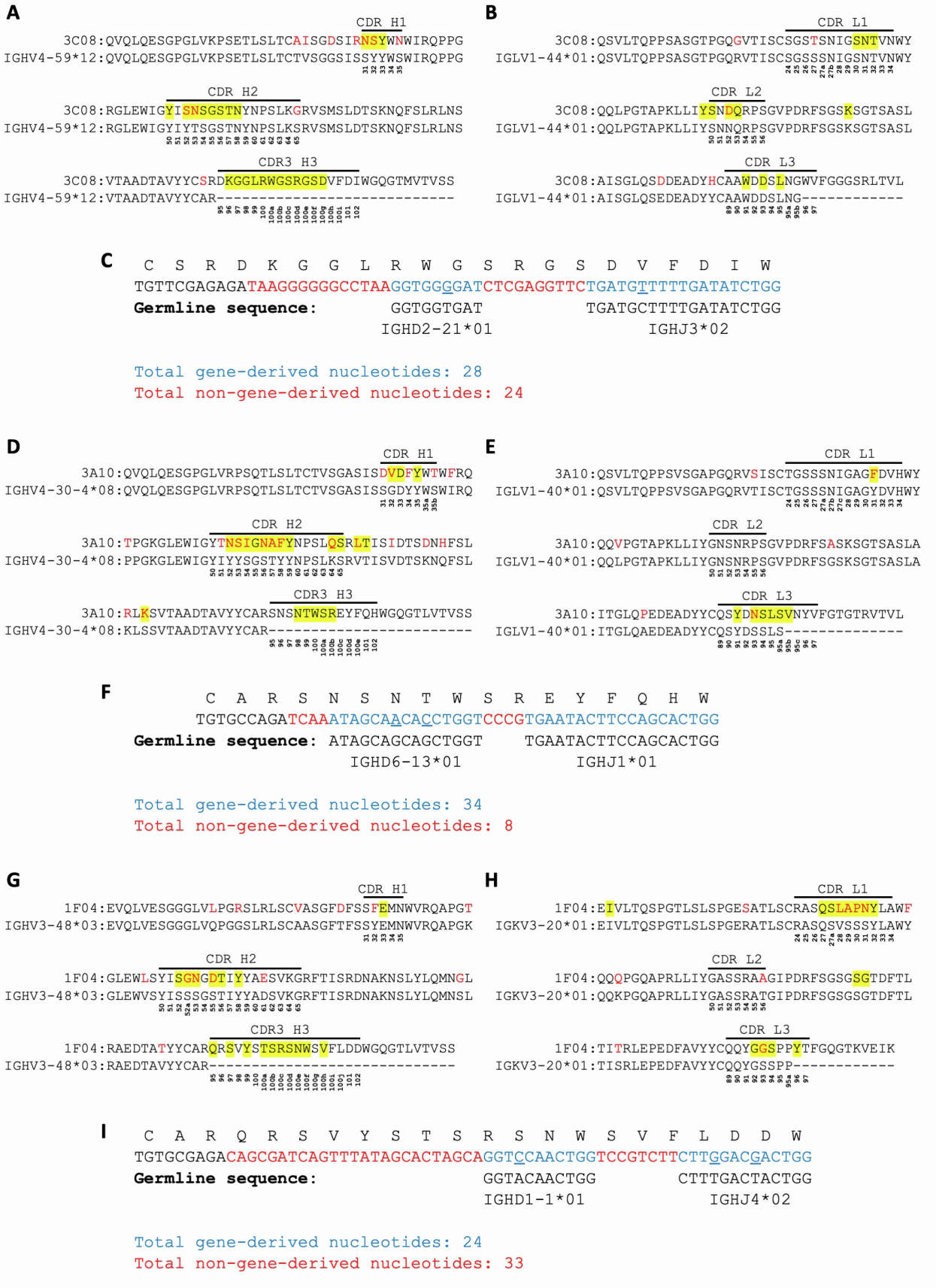
A
CDR H1
3C08:QVQLQESGPGLVKPSETLSLTCAISGDSIRNSYWNWIRQPPG
IGHV4-59*12:QVQLQESGPGLVKPSETLSLTCTVSGGSISSYYWSWIRQPPG
CDR H2
3C08:RGLEWIGYISNSGSTNYNPSLKGRVSMSLDTSKNQFSLRLNS
IGHV4-59*12:RGLEWIGYIYTSGSTNYNPSLKSRVSMSLDTSKNQFSLRLNS
CDR3 H3
3C08:VTAADTAVYYCSRDKGGLRWGSRGSDVFDIWGQGTMVTVSS
IGHV4-59*12:VTAADTAVYYCAR----------
B
CDR L1
3C08:QSVLTQPPSASGTPGQGVTISCSGSTSNIGSNTVNWY
IGLV1-44*01:QSVLTQPPSASGTPGQRVTISCSGSSSNIGSNTVNWY
CDR L2
3C08:QQLPGTAPKLLIYSNDQRPSGVPDRFSGSKSGTSASL
IGLV1-44*01:QQLPGTAPKLLIYSNNQRPSGVPDRFSGSKSGTSASL
CDR L3
3C08:AISGLQSDDEADYHCAAWDDSLNGWVFGGGSRLTVL
IGLV1-44*01:AISGLQSEDEADYYCAAWDDSLNG----------
C
C S R D K G G L R W G S R G S D V F D I W
TGTTCGAGAGATAAGGGGGGCCTAAGGTGGGGATCTCGAGGTTCTGATGTTTTTGATATCTGG
Germline sequence: GGTGGTGAT TGATGCTTTTGATATCTGG
IGHD2-21*01 IGHJ3*02
Total gene-derived nucleotides: 28
Total non-gene-derived nucleotides: 24
D
CDR H1
3A10:QVQLQESGPGLVRPSQTLSLTCTVSGASISDVDFYWTWFRQ
IGHV4-30-4*08:QVQLQESGPGLVRPSQTLSLTCTVSGASISSGDYYWSWIRQ
CDR H2
3A10:TPGKGLEWIGYTNSIGNAFYNPSLQSRLTISIDTSDNHFSL
IGHV4-30-4*08:PPGKGLEWIGYIYYSGSTYYNPSLKSRVTISVDTSKNQFSL
CDR3 H3
3A10:RLKSVTAADTAVYYCARSNSNTWSREYFQHWGQGTLVTVSS
IGHV4-30-4*08:KLSSVTAADTAVYYCAR----------
E
CDR L1
3A10:QSVLTQPPSVSGAPGQRVSISCTGSSSNIGAGFDVHWY
IGLV1-40*01:QSVLTQPPSVSGAPGQRVTISCTGSSSNIGAGYDVHWY
CDR L2
3A10:QQVPGTAPKLLIYGNSNRPSGVPDRFSASKSGTSASLA
IGLV1-40*01:QQLPGTAPKLLIYGNSNRPSGVPDRFSGSKSGTSASLA
CDR L3
3A10:ITGLQPEDEADYYCQSYDNSLSVNYVFGTGTRVTVL
IGLV1-40*01:ITGLQAEDEADYYCQSYDSSLS----------
F
C A R S N S N T W S R E Y F Q H W
TGTGCCAGATCAAATAGCAACACCTGGTCCCGTGAATACTTCCAGCACTGG
Germline sequence: ATAGCAGCAGCTGGT TGAATACTTCCAGCACTGG
IGHD6-13*01 IGHJ1*01
Total gene-derived nucleotides: 34
Total non-gene-derived nucleotides: 8
G
CDR H1
1F04:EVQLVESGGGLVLPGRSLRLSCVASGFDFSSFEMNWVRQAPGT
IGHV3-48*03:EVQLVESGGGLVQPGGSLRLSCAASGFTFSSYEMNWVRQAPGK
CDR H2
1F04:GLEWLSYISGNGDTIYYAESVKGRFTISRDNAKNSLYLQMNGL
IGHV3-48*03:GLEWVSYISSSGSTIYYADSVKGRFTISRDNAKNSLYLQMNSL
CDR3 H3
1F04:RAEDTATYYCARQRSVYSTSRSNWSVFLDDWGQGTLVTVSS
IGHV3-48*03:RAEDTAVYYCAR----------
H
CDR L1
1F04:EIVLTQSPGTLSLSPGESATLSCRASQSLAPNYLAWF
IGKV3-20*01:EIVLTQSPGTLSLSPGERATLSCRASQSVSSSYLAWY
CDR L2
1F04:QQQPGQAPRLLIYGASSRAAGIPDRFSGSGSGTDFTL
IGKV3-20*01:QQKPGQAPRLLIYGASSRATGIPDRFSGSGSGTDFTL
CDR L3
1F04:TITRLEPEDFAVYYCQQYGGSPPYTFGQGTKVEIK
IGKV3-20*01:TISRLEPEDFAVYYCQQYGSSPP----------
I
C A R Q R S V Y S T S R S N W S V F L D D W
TGTGCGAGACAGCGATCAGTTTATAGCACTAGCAGGTCCAACTGGTCCGTCTTCTTGGACGACTGG
Germline sequence: GGTACAACTGG CTTTGACTACTGG
IGHD1-1*01 IGHJ4*02
Total gene-derived nucleotides: 24
Total non-gene-derived nucleotides: 33

Figure S2. Comparison of 3C08, 3A10, and 1F04 sequence to their putative germline sequences, Related to Figure 2. (A, D, G) Alignment of the heavy-chain variable domain sequences of **(A)** 3C08, **(D)** 3A10, and **(G)** 1F04 with their corresponding germline sequences. **(B, E, H)** Alignment of the light-chain variable domain sequences **(B)** 3C08, **(E)** 3A10, and **(H)** 1F04 with their corresponding germline sequences. Regions that correspond to CDR H1, H2, H3, L1, L2, and L3 are indicated. Residues that differ from the germline are highlighted in red. Residue positions in the CDRs are labeled according to the Kabat numbering scheme. Antibody residues that interact with NA are highlighted in yellow. **(C, F, I)** Sequences of the V-D-J junctions of **(C)** 3C08, **(F)** 3A10, and **(I)** 1F04 are shown with putative D and V gene segments as well as N-regions indicated. Somatically mutated nucleotides are underlined.

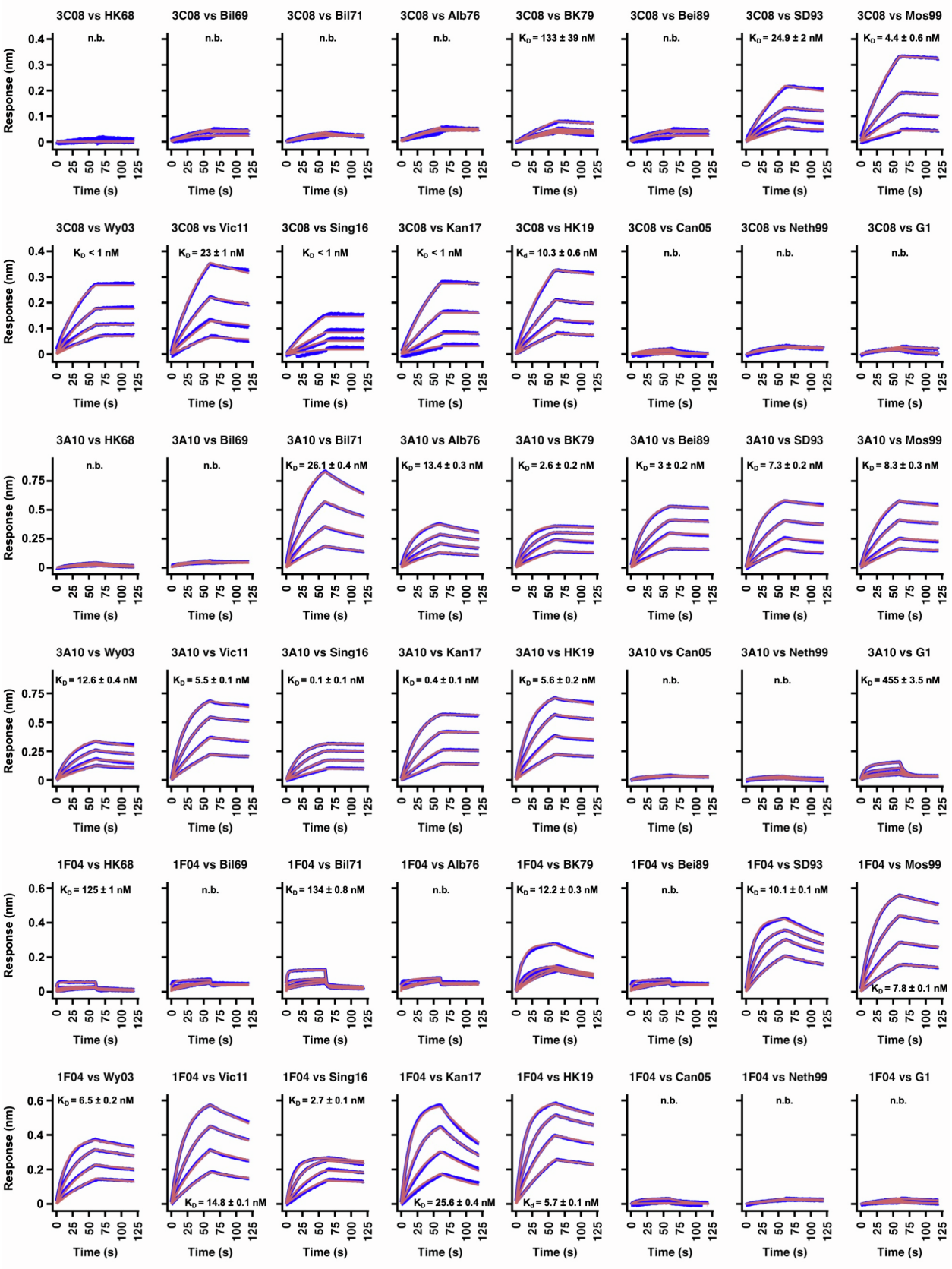
3C08 vs HK68
n.b.
3C08 vs Bil69
n.b.
3C08 vs Bil71
n.b.
3C08 vs Alb76
n.b.
3C08 vs BK79
K_D = 133 ± 39 nM
3C08 vs Bei89
n.b.
3C08 vs SD93
K_D = 24.9 ± 2 nM
3C08 vs Mos99
K_D = 4.4 ± 0.6 nM
3C08 vs Wy03
K_D < 1 nM
3C08 vs Vic11
K_D = 23 ± 1 nM
3C08 vs Sing16
K_D < 1 nM
3C08 vs Kan17
K_D < 1 nM
3C08 vs HK19
K_d = 10.3 ± 0.6 nM
3C08 vs Can05
n.b.
3C08 vs Neth99
n.b.
3C08 vs G1
n.b.
3A10 vs HK68
n.b.
3A10 vs Bil69
n.b.
3A10 vs Bil71
K_D = 26.1 ± 0.4 nM
3A10 vs Alb76
K_D = 13.4 ± 0.3 nM
3A10 vs BK79
K_D = 2.6 ± 0.2 nM
3A10 vs Bei89
K_D = 3 ± 0.2 nM
3A10 vs SD93
K_D = 7.3 ± 0.2 nM
3A10 vs Mos99
K_D = 8.3 ± 0.3 nM
3A10 vs Wy03
K_D = 12.6 ± 0.4 nM
3A10 vs Vic11
K_D = 5.5 ± 0.1 nM
3A10 vs Sing16
K_D = 0.1 ± 0.1 nM
3A10 vs Kan17
K_D = 0.4 ± 0.1 nM
3A10 vs HK19
K_D = 5.6 ± 0.2 nM
3A10 vs Can05
n.b.
3A10 vs Neth99
n.b.
3A10 vs G1
K_D = 455 ± 3.5 nM
1F04 vs HK68
K_D = 125 ± 1 nM
1F04 vs Bil69
n.b.
1F04 vs Bil71
K_D = 134 ± 0.8 nM
1F04 vs Alb76
n.b.
1F04 vs BK79
K_D = 12.2 ± 0.3 nM
1F04 vs Bei89
n.b.
1F04 vs SD93
K_D = 10.1 ± 0.1 nM
1F04 vs Mos99
K_D = 7.8 ± 0.1 nM
1F04 vs Wy03
K_D = 6.5 ± 0.2 nM
1F04 vs Vic11
K_D = 14.8 ± 0.1 nM
1F04 vs Sing16
K_D = 2.7 ± 0.1 nM
1F04 vs Kan17
K_D = 25.6 ± 0.4 nM
1F04 vs HK19
K_d = 5.7 ± 0.1 nM
1F04 vs Can05
n.b.
1F04 vs Neth99
n.b.
1F04 vs G1
n.b.
Response (nm)
Time (s)

Figure S3. Sensorgrams for binding of Fabs to NAs, Related to Table 1. Binding kinetics of 3C10, 3A10, and 1F04 Fabs against the indicated recombinant NA proteins by biolayer interferometry (BLI) are shown. Y-axis represents the response. Blue lines represent the response curve and red lines represent the best fit model (1:1 binding model or 2:1 heterogeneous ligand model, see STAR Methods). Binding kinetics were measured for four concentrations of Fab at 2-fold dilution ranging from 200 nM to 25 nM. Dissociation constants (K_D), if shown, indicate mean ± standard deviation. n.b.: no binding.

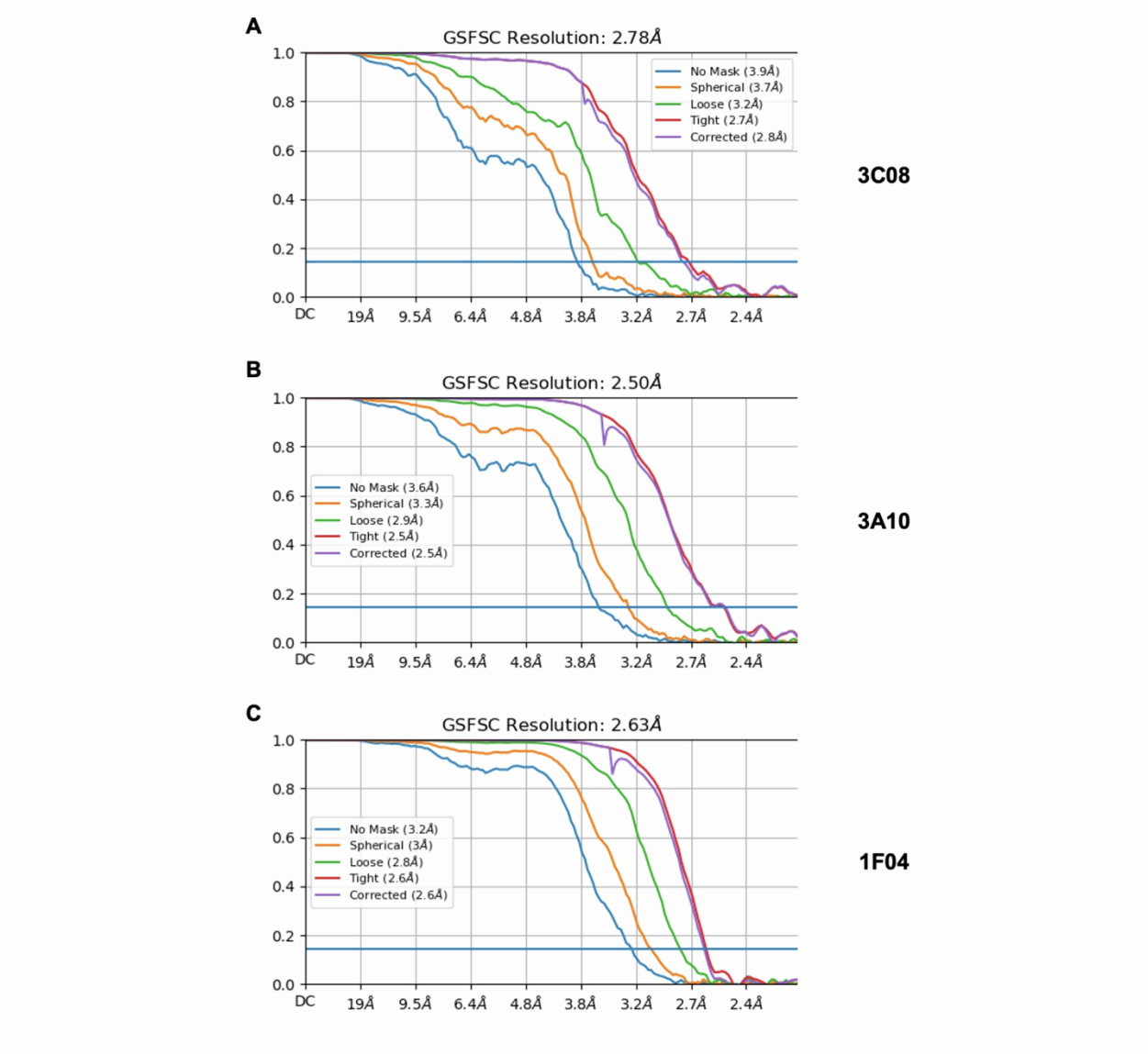

Figure S4. Cryo-EM structure validation and analysis, Related to Figure 1. Gold-standard Fourier shell correlation (GSFSC) curves of **(A)** 3C08 in complex with Mos99 NA, **(B)** 3A10 in complex with Mos99 NA, and **(C)** 1F04 in complex with Mos99 NA.

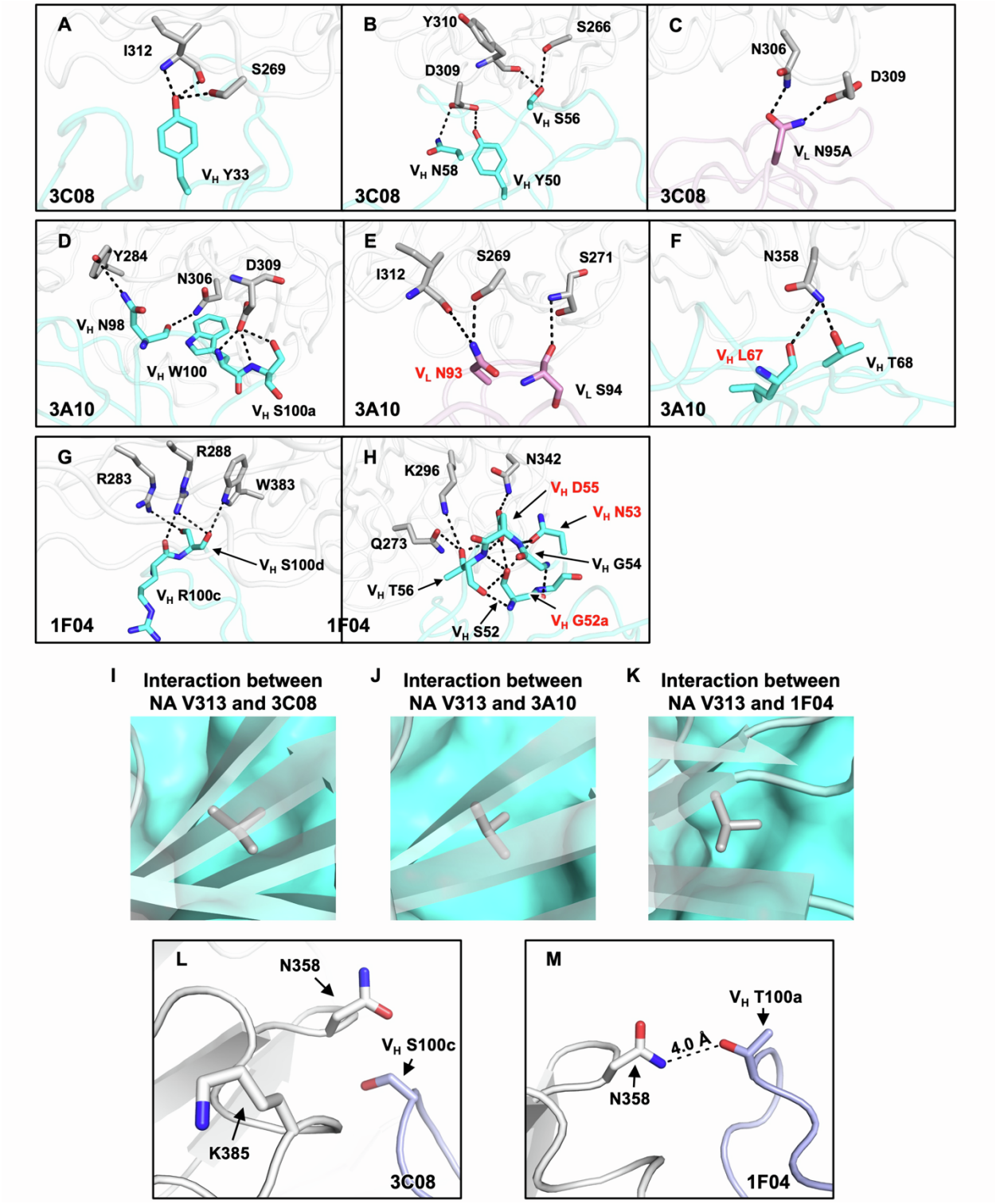

Figure S5. Interactions between the NA and antibodies, Related to Figure 2. Interactions of NA and key paratope residues in **(A)** CDR H1 of 3C08, **(B)** CDR H2 of 3C08, **(C)** CDR L3 of 3C08, **(D)** CDR H3 of 3A10, **(E)** CDR L3 of 3A10, **(F)** framework region 3 of 3A10, **(G)** V_H R100c of 1F04,

and **(H)** CDR H2 of 1F04 are shown. For each antibody, heavy chain is colored in cyan, whereas light chain is in pink. NA is colored in gray. H-bonds are shown as black dashed lines. Residues that represent somatic hypermutations are labeled in red. **(I-K)** Interaction between NA V313 and each antibody is shown. NA is colored in gray with the backbone shown as semitransparent cartoon representation and the side chain of residue 313 as sticks representation. Antibodies, namely **(I)** 3C08, **(J)** 3A10, and **(K)** 1F04, are shown as cyan surface. **(L)** The side chains of NA N358 and K385 as well as 3C08 V_H S100c are shown as sticks representation. **(M)** The side chains of NA N358 and 1F04 V_H T100a are shown as sticks representation. NA is colored in white, whereas heavy chain of the antibody is in light blue.

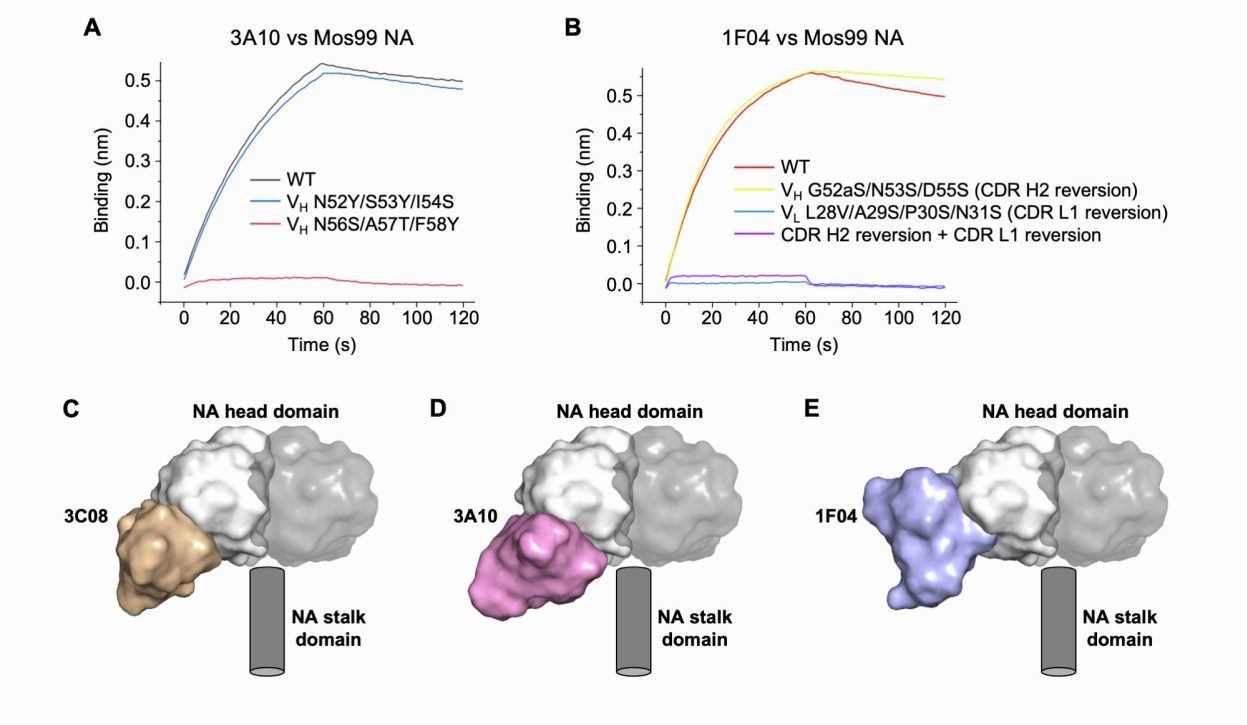

Figure S6. Additional characterization of 3C08, 3A10, and 1F04, Related to Figure 2. (A-B) Binding kinetics of **(A)** 3C10 WT and the indicated germline-reversion mutants, as well as **(B)** 1F04 WT and the indicated germline-reversion mutants against Mos99 NA. Y-axis represents the response. All Fabs were tested at 200 nM. **(C-E)** The location of the NA stalk domain is indicated on the cryo-EM structures of NA in complex with **(C)** 3C08 Fab, **(D)** 3A10 Fab, and **(E)** 1F04 Fab. For clarity, only the variable region of one Fab is displayed in each tetrameric structure. The NA is in surface representation with one protomer colored in white and the other three in dark gray.

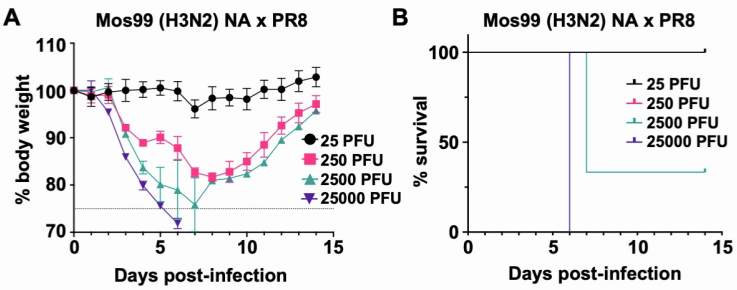

Figure S7. Determining the LD_{50} for the Mos99 NA x PR8 recombinant virus, Related to Figure 5 and Figure 6. 6-week-old female BALB/c mice (n = 3 per group) were infected intranasally with the indicated doses of recombinant N2/Mos99 virus (7:1 on backbone from A/Puerto Rico/8/1934). **(A)** Body weight, and **(B)** survival were monitored for 14 days.

SUPPLEMENTAL REFERENCES

S1. Wang, F., Wan, Z., Wu, J., Wang, Y., Fu, H., Shao, H., Qian, K., Gao, W., Ye, J., and Qin, A. (2021). A cross-reactive monoclonal antibody against neuraminidases of both H9N2 and H3N2 influenza viruses shows protection in mice challenging models. Front Microbiol *12*, 730449. 10.3389/fmicb.2021.730449.

S2. Gulati, U., Hwang, C.C., Venkatramani, L., Gulati, S., Stray, S.J., Lee, J.T., Laver, W.G., Bochkarev, A., Zlotnick, A., and Air, G.M. (2002). Antibody epitopes on the neuraminidase of a recent H3N2 influenza virus (A/Memphis/31/98). J Virol *76*, 12274-12280.

S3. DeDiego, M.L., Chiem, K., and Topham, D.J. (2018). Directed selection of amino acid changes in the influenza hemagglutinin and neuraminidase affecting protein antigenicity. Vaccine *36*, 6383-6392. 10.1016/j.vaccine.2018.09.005.

S4. Kirkpatrick Roubidoux, E., McMahon, M., Carreno, J.M., Capuano, C., Jiang, K., Simon, V., van Bakel, H., Wilson, P., and Krammer, F. (2021). Identification and characterization of novel antibody epitopes on the N2 neuraminidase. mSphere *6*, e00958-20. 10.1128/mSphere.00958-20.

S5. Wan, Z., Ye, J., Sang, J., Shao, H., Qian, K., Jin, W., Qin, A., and Wan, H. (2016). Identification of amino acids in H9N2 influenza virus neuraminidase that are critical for the binding of two mouse monoclonal antibodies. Vet Microbiol *187*, 58-63. 10.1016/j.vetmic.2016.03.011.

S6. Chen, Y.Q., Wohlbold, T.J., Zheng, N.Y., Huang, M., Huang, Y., Neu, K.E., Lee, J., Wan, H., Rojas, K.T., Kirkpatrick, E., et al. (2018). Influenza infection in humans induces broadly cross-reactive and protective neuraminidase-reactive antibodies. Cell *173*, 417-429.e10. 10.1016/j.cell.2018.03.030.

S7. Wan, H., Gao, J., Yang, H., Yang, S., Harvey, R., Chen, Y.Q., Zheng, N.Y., Chang, J., Carney, P.J., Li, X., et al. (2019). The neuraminidase of A(H3N2) influenza viruses circulating since 2016 is antigenically distinct from the A/Hong Kong/4801/2014 vaccine strain. Nat Microbiol *4*, 2216-2225. 10.1038/s41564-019-0522-6.

S8. Doyle, T.M., Hashem, A.M., Li, C., Van Domselaar, G., Larocque, L., Wang, J., Smith, D., Cyr, T., Farnsworth, A., He, R., et al. (2013). Universal anti-neuraminidase antibody inhibiting all influenza A subtypes. Antiviral Res *100*, 567-574. 10.1016/j.antiviral.2013.09.018.

S9. Tulip, W.R., Varghese, J.N., Laver, W.G., Webster, R.G., and Colman, P.M. (1992). Refined crystal structure of the influenza virus N9 neuraminidase-NC41 Fab complex. J Mol Biol *227*, 122-148. 10.1016/0022-2836(92)90687-f.

S10. Tulip, W.R., Varghese, J.N., Webster, R.G., Laver, W.G., and Colman, P.M. (1992). Crystal structures of two mutant neuraminidase-antibody complexes with amino acid substitutions in the interface. J Mol Biol *227*, 149-159. 10.1016/0022-2836(92)90688-g.

S11. Tulip, W.R., Harley, V.R., Webster, R.G., and Novotny, J. (1994). N9 neuraminidase complexes with antibodies NC41 and NC10: empirical free energy calculations capture

specificity trends observed with mutant binding data. Biochemistry *33*, 7986-7997. 10.1021/bi00192a002.

S12. Malby, R.L., Tulip, W.R., Harley, V.R., McKimm-Breschkin, J.L., Laver, W.G., Webster, R.G., and Colman, P.M. (1994). The structure of a complex between the NC10 antibody and influenza virus neuraminidase and comparison with the overlapping binding site of the NC41 antibody. Structure *2*, 733-746.

S13. Malby, R.L., McCoy, A.J., Kortt, A.A., Hudson, P.J., and Colman, P.M. (1998). Three-dimensional structures of single-chain Fv-neuraminidase complexes. J Mol Biol *279*, 901-910. 10.1006/jmbi.1998.1794.

S14. Venkatramani, L., Bochkareva, E., Lee, J.T., Gulati, U., Graeme Laver, W., Bochkarev, A., and Air, G.M. (2006). An epidemiologically significant epitope of a 1998 human influenza virus neuraminidase forms a highly hydrated interface in the NA-antibody complex. J Mol Biol *356*, 651-663. 10.1016/j.jmb.2005.11.061.

S15. Wan, H., Yang, H., Shore, D.A., Garten, R.J., Couzens, L., Gao, J., Jiang, L., Carney, P.J., Villanueva, J., Stevens, J., and Eichelberger, M.C. (2015). Structural characterization of a protective epitope spanning A(H1N1)pdm09 influenza virus neuraminidase monomers. Nat Commun *6*, 6114. 10.1038/ncomms7114.

S16. Zhu, X., Turner, H.L., Lang, S., McBride, R., Bangaru, S., Gilchuk, I.M., Yu, W., Paulson, J.C., Crowe, J.E., Jr., Ward, A.B., and Wilson, I.A. (2019). Structural basis of protection against H7N9 influenza virus by human anti-N9 neuraminidase antibodies. Cell Host Microbe *26*, 729-738.e4. 10.1016/j.chom.2019.10.002.

S17. Stadlbauer, D., Zhu, X., McMahon, M., Turner, J.S., Wohlbold, T.J., Schmitz, A.J., Strohmeier, S., Yu, W., Nachbagauer, R., Mudd, P.A., et al. (2019). Broadly protective human antibodies that target the active site of influenza virus neuraminidase. Science *366*, 499-504. 10.1126/science.aay0678.

S18. Jiang, H., Peng, W., Qi, J., Chai, Y., Song, H., Bi, Y., Rijal, P., Wang, H., Oladejo, B.O., Liu, J., et al. (2020). Structure-based modification of an anti-neuraminidase human antibody restores protection efficacy against the drifted influenza virus. mBio *11*, e02315-20. 10.1128/mBio.02315-20.

S19. Madsen, A., Dai, Y.N., McMahon, M., Schmitz, A.J., Turner, J.S., Tan, J., Lei, T., Alsoussi, W.B., Strohmeier, S., Amor, M., et al. (2020). Human antibodies targeting influenza B virus neuraminidase active site are broadly protective. Immunity *53*, 852-863.e7. 10.1016/j.immuni.2020.08.015.